Research article

NMR IN BIOMEDICINE

Received: 28 February 2014, Revised: 11 May 2014, Accepted: 5 June 2014, Published online in Wiley Online Library

(wileyonlinelibrary.com) DOI: 10.1002/nbm.3160

Cerebral blood volume estimation by ferumoxytol-enhanced steady-state MRI at 9.4 T reveals microvascular impact of α_1-adrenergic receptor antibodies

Andreas Pohlmann[a]*†, Peter Karczewski[b†], Min-Chi Ku[a], Babette Dieringer[a], Helmar Waiczies[a,c], Natali Wisbrun[d], Stefanie Kox[a], Irina Palatnik[a], Henning Matthias Reimann[a], Christina Eichhorn[e], Sonia Waiczies[a,c], Petra Hempel[b], Bernd Lemke[b], Thoralf Niendorf[a,c‡] and Marion Bimmler[f‡]

Cerebrovascular abnormality is frequently accompanied by cognitive dysfunctions, such as dementia. Antibodies against the α_1-adrenoceptor (α_1-AR) can be found in patients with Alzheimer's disease with cerebrovascular disease, and have been shown to affect the larger vessels of the brain in rodents. However, the impact of α_1-AR antibodies on the cerebral vasculature remains unclear. In the present study, we established a neuroimaging method to measure the relative cerebral blood volume (rCBV) in small rodents with the ultimate goal to detect changes in blood vessel density and/or vessel size induced by α_1-AR antibodies. For this purpose, mapping of R_2* and R_2 was performed using MRI at 9.4 T, before and after the injection of intravascular iron oxide particles (ferumoxytol). The change in the transverse relaxation rates (ΔR_2*, ΔR_2) showed a significant rCBV decrease in the cerebrum, cortex and hippocampus of rats (except hippocampal ΔR_2), which was more pronounced for ΔR_2* than for ΔR_2. Immunohistological analyses confirmed that the α_1-AR antibody induced blood vessel deficiencies. Our findings support the hypothesis that α_1-AR antibodies lead to cerebral vessel damage throughout the brain, which can be monitored by MRI-derived rCBV, a non-invasive neuroimaging method. This demonstrates the value of rCBV estimation by ferumoxytol-enhanced MRI at 9.4 T, and further underlines the significance of this antibody in brain diseases involving vasculature impairments, such as dementia. Copyright © 2014 John Wiley & Sons, Ltd.

Additional supporting information may be found in the online version of this article at the publisher's web site.

Keywords: MRI; cerebral blood volume (CBV); ferumoxytol; ultrasmall superparamagnetic iron oxide (USPIO); α_1-adrenergic receptor antibody; rat

INTRODUCTION

Cerebrovascular disease, a group of pathological processes affecting the small arteries, arterioles, venules and capillaries of the brain (1), is frequently accompanied by cognitive dysfunction. Although it remains challenging to determine the contribution of cerebrovascular disease to cognitive impairment, or vice versa, accumulating evidence indicates that cerebrovascular disease might be an important cause of cognitive dysfunction and neurodegeneration,

* *Correspondence to: A. Pohlmann, Max Delbrück Center for Molecular Medicine, Robert Rössle Str. 10, 13125 Berlin, Germany. E-mail: andreas.pohlmann@mdc-berlin.de*

a *A. Pohlmann, M.-C. Ku, B. Dieringer, H. Waiczies, S. Kox, I. Palatnik, H. M. Reimann, S. Waiczies, T. Niendorf*
Berlin Ultrahigh Field Facility (B.U.F.F.), Max Delbrück Center for Molecular Medicine, Berlin, Germany

b *P. Karczewski, P. Hempel, B. Lemke*
E.R.D.E.-AAK-Diagnostik GmbH, Berlin, Germany

c *H. Waiczies, S. Waiczies, T. Niendorf*
Experimental and Clinical Research Center, a joint cooperation between the Charité Medical Faculty and the Max Delbrück Center for Molecular Medicine, Berlin, Germany

d *N. Wisbrun*
Leibniz Institut for Molecular Pharmacology im Forschungsverbund Berlin, Germany

e *C. Eichhorn*
Statistical Sciences, Department of Information Technology, Max Delbrück Center for Molecular Medicine, Berlin, Germany

f *M. Bimmler*
Autoimmunity and G Protein-Coupled Receptors, Max Delbrück Center for Molecular Medicine, Berlin, Germany

† *These authors contributed equally to this work.*

‡ *These authors contributed equally to this work.*

Abbreviations used: *α_1-AR, α_1-adrenoceptor; AD, Alzheimer's disease; CBV, cerebral blood volume; CVR, cerebrovascular reactivity; IgG, immunoglobulin G; MGE, multigradient echo; MSME, multislice multispin echo; rCBV, relative cerebral blood volume; RF, radiofrequency; SEM, standard error of the mean; USPIO, ultrasmall superparamagnetic iron oxide; VOI, volume of interest.*

such as dementia (2). The findings of structural and functional changes of cerebral blood vessels suggest that brain microcirculation abnormalities might contribute to Alzheimer's disease (AD) (3). Clinical studies focusing on cerebrovascular pathologies have shown that autoantibodies against the α_1-adrenoceptor (α_1-AR) with agonist-like activity can be found in patients with hypertension (4,5), as well as in patients with AD with cerebrovascular disease (6), suggesting that the observed vascular symptoms might be induced by the α_1-AR antibody (7,8). α_1-AR is a member of the G-protein-coupled receptor superfamily which mediates the physiological responses to norepinephrine and epinephrine, which regulate several important cardiovascular actions (9), and has been found to be expressed on human cerebral blood vessels (10). Vascular impairments in the larger vessels of the rat brain after exposure to the α_1-AR antibody have been shown recently by time-of-flight MR angiography (11). However, this approach is not able to depict blood vessels significantly smaller in diameter than the spatial resolution – 100 μm in this study – so that the impact of α_1-AR on the cerebral vasculature, in particular the microvasculature down to the capillary level, is still unknown. Realizing the challenges and opportunities of probing for subtle cerebrovascular changes in experimental *in vivo* models, it is conceptually appealing to pursue non-invasive cerebral blood volume (CBV) mapping techniques that allow for longitudinal *in vivo* studies.

MRI enables the non-invasive estimation of the relative cerebral blood volume (rCBV) and hence the detection of changes in blood vessel density and/or vessel size. Tracking the signal intensity–time curve during bolus injection of gadolinium-based contrast agents is the clinical standard for rCBV assessment (12). This approach requires MRI with high temporal resolution and inherently limited spatial resolution. If the blood–brain barrier is compromised, leakage of the contrast agent into the interstitium can be a confounding factor (13). Intravascular contrast agents, such as ultrasmall superparamagnetic iron oxides (USPIOs), represent an attractive alternative for rCBV assessment with MRI (14). The long plasma half-life and tendency to remain intravascular of USPIO facilitates steady-state measurements, yielding more accurate rCBV estimation (15,16). For rCBV estimation pre-/post-contrast, changes in the effective transverse relaxation rate (R_2*) are used, assuming a linear dependence of R_2* on the USPIO blood plasma concentration (ΔR_2* ~ rCBV) (17–19).

Lately, the (pre-)clinical use of USPIOs as MRI contrast agents is being hindered by the unavailability of various commercial USPIOs (e.g. Resovist®, Feridex®/Endorem®, Combidex®/Sinerem® have been discontinued), leaving no Food and Drug Administration (FDA)-approved USPIO contrast agent available for clinical MRI (20). Ferumoxytol (Feraheme®) is a USPIO that has been FDA approved as an intravenous iron supplement for the treatment of anemia in patients with chronic kidney disease (21). Ferumoxytol's non-toxicity, even at high doses, and long blood plasma half-life of approximately 15 h in humans (Feraheme® injection label, FDA) and >2 h in rats (20,22) make it well suited as an intravascular MRI contrast agent. To date ferumoxytol's potential for rCBV measurements remains largely untapped, with only a few reports of its use in humans (13,23–26) and small rodents (16,27,28). Despite its early application in rat brain MRI (29), ferumoxytol-enhanced rCBV measurements at the common pre-clinical MRI system field strength of 9.4 T have not been reported to date.

In this work, we aimed to establish the feasibility of rCBV monitoring in rats by ferumoxytol-enhanced MRI at 9.4 T and to demonstrate, for the first time, α_1-AR antibody-induced cerebral microvascular impairments by the application of this technique. Analysis of ΔR_2* and ΔR_2 showed a significant decrease in rCBV in the cerebrum, cortex and hippocampus in rats, suggesting a strong impact of α_1-AR antibodies on the cerebral microvasculature.

MATERIALS AND METHODS

Animal model

Male Wistar rats (10–13 weeks of age; 280–350 g) were purchased from Charles River Laboratories, Sulzfeld, Germany. All animal experiments were approved and carried out in accordance with the regulation and guidelines provided by the Animal Welfare Department of the Landesamt für Gesundheit und Soziales Berlin (Berlin State Office of Health and Social Affairs, Permit Number: G0197/10). Eighteen rats were randomly allocated to two experimental groups, with nine rats in each. One group received intravenous injections of α_1-AR antibodies (700 mg/kg body weight), prepared as described in ref. (11). The corresponding control group was injected with the same dose of control immunoglobulin G (IgG). The injections were repeated monthly. To measure the antibody concentration, blood serum was obtained as described previously (11). All rats were anesthetized by inhalation of isoflurane in air throughout the entire imaging experiment.

Ferumoxytol particle size analysis and dose optimization

In vitro analysis of ferumoxytol and *in vivo* pilot MRI measurements were carried out to establish the suitability of ferumoxytol for off-label use as an intravascular MRI contrast agent for rat CBV monitoring at 9.4 T. As the magnetic properties of USPIOs depend on their particle size, production batches with different particle sizes may have different magnetic properties (14). In order to determine the particle size variability between batches of ferumoxytol, particle size analysis of samples taken from three separately purchased 17-mL Feraheme® vials (AMAG Pharmaceuticals, Inc., Lexington, MA, USA) was performed by dynamic light scattering (Malvern Zetasizer Nano ZS instrument, Malvern Instruments, Malvern, Worcestershire, UK).

To determine a ferumoxytol dose suitable for rat rCBV measurements at 9.4 T, initial titration experiments were performed in two animals for dose calibration. Following baseline T_2 and T_2* mapping, four consecutive doses of 5 mg of Fe/kg ferumoxytol (Feraheme®, AMAG Pharmaceuticals, Inc.) were administered using a power injector at an infusion rate of 0.25 mL/min via a tail vein catheter. Parametric mapping was repeated after each injection, i.e. at 5, 10, 15 and 20 mg of Fe/kg ferumoxytol.

The time courses of T_2*, T_2 and T_2-weighted image intensity were monitored in two animals for approximately 100 min following a single dose of 10 mg of Fe/kg ferumoxytol to confirm a sufficiently slow temporal change in plasma concentration that allows for post-injection T_2 and T_2* mapping during a period of approximately 15 min after contrast agent administration.

Study design

Eighteen rats underwent MRI at 9 and 11 months after treatment (α_1-AR antibodies or IgG) had commenced. Following baseline T_2 and T_2* mapping, 10 mg of Fe/kg ferumoxytol (Feraheme®, AMAG Pharmaceuticals, Inc.) was administered using a power

injector at a rate of 0.25 mL/min via a tail vein catheter. Following a 3-min mixing time starting from the end of injection, T_2 and T_2* mapping was repeated.

MRI

Animals were anesthetized with isoflurane (1.8–2.0% in air), the tail vein was catheterized and the animal was transferred to the warmed animal holder of a horizontal 9.4-T small-bore (20-cm) animal MR system (Biospec 94/20, Bruker Biospin, Ettlingen, Germany). The MR system was equipped with a linear polarized birdcage radiofrequency (RF) resonator for transmission, in conjunction with a curved four-channel receive RF coil array (Bruker Biospin) customized for rat brain imaging.

T_2* mapping used a multigradient echo (MGE) sequence (TR = 620 ms; TEs = 8; first TE = 2.14 ms; TE increment = 2.14 ms; averages, 2; positive spoiler gradient of 20% strength and 1.43 ms in duration) with a total acquisition time of 4 min. TEs were chosen to be integral multiples of 0.7137 ms at which water and fat are in phase (based on the measured fat–water frequency shift). For T_2 mapping, a multislice multispin echo (MSME) sequence (TR = 2000 ms; TEs = 7; first TE = 9.99 ms; TE increment = 9.99 ms; positive spoiler gradient of 20% strength and 0.5 ms in duration) was employed, with a total acquisition time of 6 min. For T_2* and T_2 mapping, 21 consecutive coronal slices covering the entire brain were acquired with an in-plane spatial resolution of (137×137) μm^2, field of view of (35×35) mm^2, matrix size of 256×256 and slice thickness of 1.0 mm.

Image analysis

Parametric maps of absolute T_2* and T_2 were calculated by pixel-wise mono-exponential fitting to the signal intensities of denoised series (SANLM filter, VBM8 toolbox, SPM8, www.fil.ion.ucl.ac.uk/spm) of T_2*- and T_2-weighted images acquired as a function of TE (in-house developed program; MATLAB, R2010a, MathWorks, Natick, WA, USA). Relaxation times T_2* and T_2 were converted to their corresponding relaxivities, $R_2^* = 1/T_2^*$ and $R_2 = 1/T_2$, and subtraction of pre-contrast maps from post-contrast maps yielded parametric ΔR_2* and ΔR_2 maps.

Volume of interest (VOI) analysis using ImageJ (National Institutes of Health, Bethesda, MD, USA; http://imagej.nih.gov/ij) was performed on all datasets for which: (i) it was certain that the entire target volume of ferumoxytol had been injected intravenously; and (ii) the parametric mapping yielded brain tissue T_2* (T_2) values in the range 1–50 ms (10–100 ms). For all animals, the cerebrum was extracted by manual segmentation of all 21 coronal slices using the longest TE image (TE_{MSME} = 69.93 ms, TE_{MGE} = 17.12 ms). This was followed by an automated division of each segmented brain map into dorsal and ventral halves. Further quantitative analysis was applied only to the dorsal brain half, hence excluding ventral brain regions that were influenced by macroscopic susceptibility artifacts originating from ventral cavities outside the brain. In addition to the dorsal cerebrum, two further VOIs were defined by manual segmentation of the cortex and hippocampus, based on pre-contrast T_2-weighted images (TE_{MSME} = 69.93 ms) and post-contrast T_2*-weighted images (TE_{MGE} = 6.42 ms), respectively.

Histograms of ΔR_2* and ΔR_2 were obtained from the parametric maps generated for each VOI and animal. Histogram counts were averaged over the animals in each group [mean ± standard error of the mean (SEM)], after normalization (division by total number of counts, multiplication by 10 000), eliminating the dependence on the number of voxels within each VOI. Plots of the empirical cumulative frequency were used instead of common histograms, as they make shifts in the ΔR_2^* (ΔR_2) distributions towards lower/higher values more apparent. Cumulative frequency plots can be interpreted as integrals of histograms, and their frequencies range from '0' to '1' (equivalent to 100%).

For quantitative comparison between two parameter distributions (α_1-AR antibody group *versus* control group), the supremum of the absolute differences was derived from the cumulative frequencies (F_c): $d_{max} = \sup|F_c(\Delta R_{2IgG}^{(*)}) - F_c(\Delta R_{2\alpha 1AR}^{(*)})|$. The parameter d_{max} is also the basis of the statistical analysis (Kolmogorov–Smirnov test).

Blood vessel immunofluorescent staining and image processing

After the final MRI time point, the deeply anesthetized rats were perfused with 0.9% NaCl, followed by 4% paraformaldehyde. Brain tissues were removed and post-fixed overnight in 4% paraformaldehyde. Dehydrated specimens were embedded in paraffin using standard methods. Paraffin sections were dewaxed, rehydrated and antigen retrieval was performed by heating sections at 98 °C in citrate buffer at pH 6.0. For the identification of cerebral blood vessels, a primary antibody against rat CD31 was added overnight at a dilution of 1 : 50 (Abcam PLC, Cambridge, UK) at 4 °C. Alexa 594-conjugated goat anti-rabbit IgG (1 : 200, Invitrogen, Carlsbad, CA, USA) was subsequently applied. The nuclei were counterstained with 4′,6-diamidino-2-phenylindole (DAPI) (Sigma-Aldrich, Seelze, Germany). Images were taken using a confocal microscope (LSM 710, Zeiss, Jena, Germany) with 10× or 20× lenses. Care was taken to select an anatomically similar cortical region for all animals.

CD31-positive-labeled blood vessel staining was quantified using ImageJ (National Institutes of Health). After thresholding of the red color channel, the fraction of CD31-positive pixels was counted, yielding the vessel area fraction. From these thresholded red channel images, we derived two further parameters as qualitative surrogates of vessel density and vessel size. Employing binary region growing (2×) to the thresholded images, disconnected positive pixels located in the vessel walls were merged into clusters/objects. Use of the 3D Objects Counter plugin for ImageJ provided the cluster count; division by the image field of view yielded the CD31 cluster density. CD31 cluster size was calculated by dividing the vessel area fraction by the CD31 cluster density.

Statistical analysis

ΔR_2* and ΔR_2 values derived from the three VOIs were statistically analyzed by testing for a significant difference in the parameter distributions using a two-sample Kolmogorov–Smirnov test, which is sensitive to differences in the location and shape of two empirical cumulative distribution functions. A probability value of less than 0.05 was considered to be significant for differences between groups.

Statistical analysis of the quantitative blood vessel immunofluorescent staining data was performed using a one-sided *t*-test, with a probability value of less than 0.05 being considered as significant.

RESULTS

Ferumoxytol particle size analysis and dose optimization

Particle size analysis of samples taken from three separately purchased 17-mL Feraheme® vials showed that ferumoxytol has an average colloidal particle size of 23.38 ± 0.37 nm (zeta-average). The particle size distribution was narrow (Fig. 1A), ranging from 10 to 70 nm with a small polydispersity index of 0.11 ± 0.02, and did not show secondary peaks in addition to the main peak depicted in Fig. 1A.

In vivo, the rat brain relaxation times T_2* and T_2 decreased rapidly with increasing dose of ferumoxytol (Fig. 1B). Owing to its non-linear dose dependence, the T_2* reduction per consecutive dose of 5 mg Fe/kg declined, and total doses of 15 and 20 mg Fe/kg only translated into modest relaxation time changes compared with 10 mg Fe/kg. As local blood plasma concentrations of ferumoxytol (c_f) are unknown, the molar relaxivities r_2* and r_2 of ferumoxytol cannot be derived from the *in vivo* observed effects on R_2* or R_2 (where, for example, $\Delta R_2 = r_2 c_f$CBV). Nevertheless, reporting the systemic dose relaxivities $r_2{*}_{SD}$ and $r_{2,SD}$ (where, for example, $\Delta R_2 = r_{2,SD} d_f$CBV) with regard to the systemically administered iron dose (d_f) may be useful for researchers interested in employing similar protocols. $r_2{*}_{SD}$ and $r_{2,SD}$ of ferumoxytol for the cortex and subcortical area were approximately $r_2{*}_{SD,cor} = 6.6\ s^{-1}\ mg^{-1}\ kg$, $r_2{*}_{SD,sub} = 6.0\ s^{-1}\ mg^{-1}\ kg$ and $r_{2,SD,cor} = 0.34\ s^{-1}\ mg^{-1}\ kg$, $r_{2,SD,sub} = 0.28\ s^{-1}\ mg^{-1}\ kg$, as derived from linear regression to R_2* (R_2) *versus* ferumoxytol dose curves (Fig. 1D), with fitting qualities of $R^2 = 1.00$, 0.98, 1.00 and 0.97, respectively.

Time courses of T_2, T_2* and the T_2-weighted signal for regions of interest in the cortex and subcortical regions are shown in Fig. 1C. During and after contrast agent injection, a strong signal intensity decrease was observed in the T_2-weighted images (ΔSI = –32% with 10 mg Fe/kg), as demonstrated in Fig. 1C for a region of interest placed in the cortex, and as illustrated in Figure 2B in comparison with Fig. 2A also for the entire coronal slice of the rat brain. Examination of the parameter maps revealed a decrease in T_2* and T_2 throughout the brain ($\Delta T_2{*}_{cortex} = -67\%$, $\Delta T_{2,cortex} = -17\%$), as demonstrated in the plots of T_2/T_2* *versus* time (Fig. 1C) and in the color-coded ΔR_2* and ΔR_2 parameter maps (Fig. 2C, F). For illustration, all 21 coronal T_2-weighted and T_2*-weighted slices derived from a rat brain after injection of 10 mg Fe/kg ferumoxytol are shown in Figs S1 and S2, respectively, together with the corresponding ΔR_2 and ΔR_2* maps. In the 100 min following contrast agent injection, $R_2{*}_{cortex}$ and $R_{2,cortex}$ increased by merely 0.18%/min and 0.03%/min, respectively.

rCBV in α_1-AR antibody-exposed animals *versus* controls

Histograms of ΔR_2* in the dorsal cerebrum at 9 months (Fig. 3A) and 11 months (Fig. 3B) after treatment began revealed that histogram counts above $\Delta R_2{*} \approx 75$ ms were decreased in the α_1-AR antibody group compared with the control group, whereas counts below $\Delta R_2{*} \approx 75$ ms were increased. This translates into a shift of ΔR_2* towards lower values, which becomes more apparent when the cumulative frequency (Fig. 3C, D) is used. At 9 months (Fig. 3C, E) and 11 months (Fig. 3D, F), ΔR_2* and ΔR_2 in the dorsal cerebrum were found to be significantly reduced for the α_1-AR antibody group in comparison with the

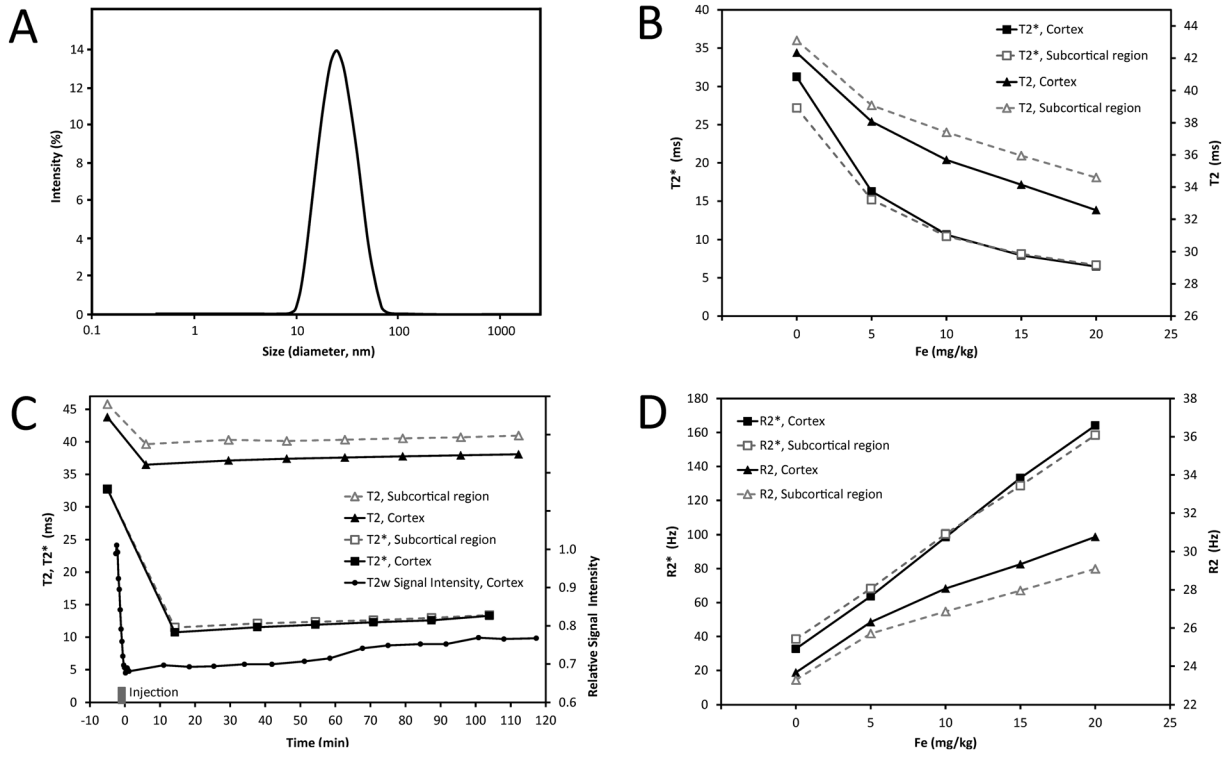

Figure 1. (A) Size distribution for a sample of ferumoxytol nanoparticles obtained from particle size analysis by dynamic light scattering. The average colloidal particle size for samples from all three vials was 23.38 ± 0.37 nm (zeta-average, logarithmic scale). (B, D) Plots of T_2*, T_2 (B) and R_2*, R_2 (D) *versus* iron dose for regions of interest placed in the cortex and subcortical regions. (C) Time courses of T_2, T_2* and the T_2-weighted (T2w) signal intensity (right axis) for regions of interest in the cortex and subcortical regions from pre-contrast to approximately 2 h after intravenous injection of 10 mg Fe/kg ferumoxytol.

NMR IN BIOMEDICINE

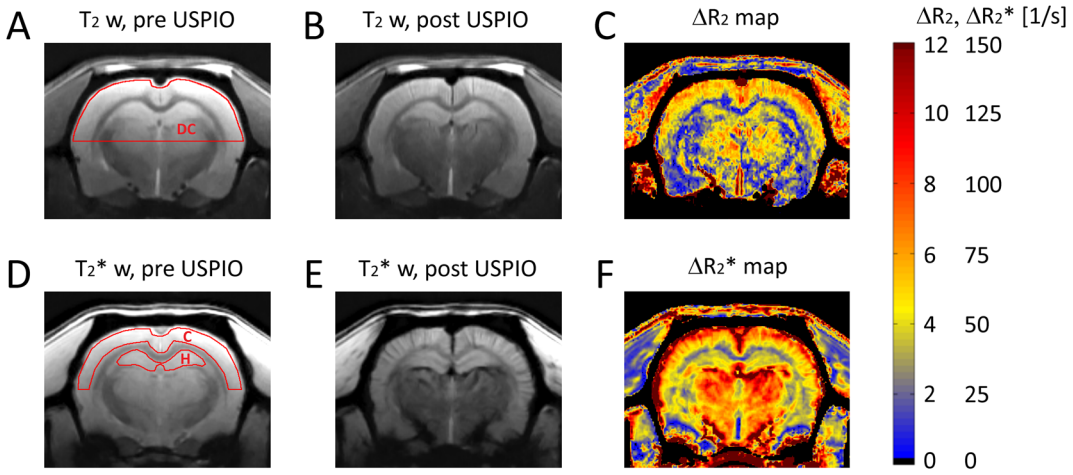

Figure 2. (A, B) Coronal T_2-weighted (T2 w) images (TE = 30 ms) of a rat brain before (A) and after (B) injection of 10 mg Fe/kg ferumoxytol. The outline of the dorsal cerebrum (DC) volume of interest (VOI) is shown in red. (C) Color-coded ΔR_2 map. (D, E) T_2*-weighted images (TE = 6.4 ms) pre-contrast (D) and post-contrast (E). The outlines of the cortex (C) and hippocampus (H) VOIs are shown in red. The vessels running into the cortex can clearly be seen in (D). (F) Color-coded ΔR_2* map. USPIO, ultrasmall superparamagnetic iron oxide.

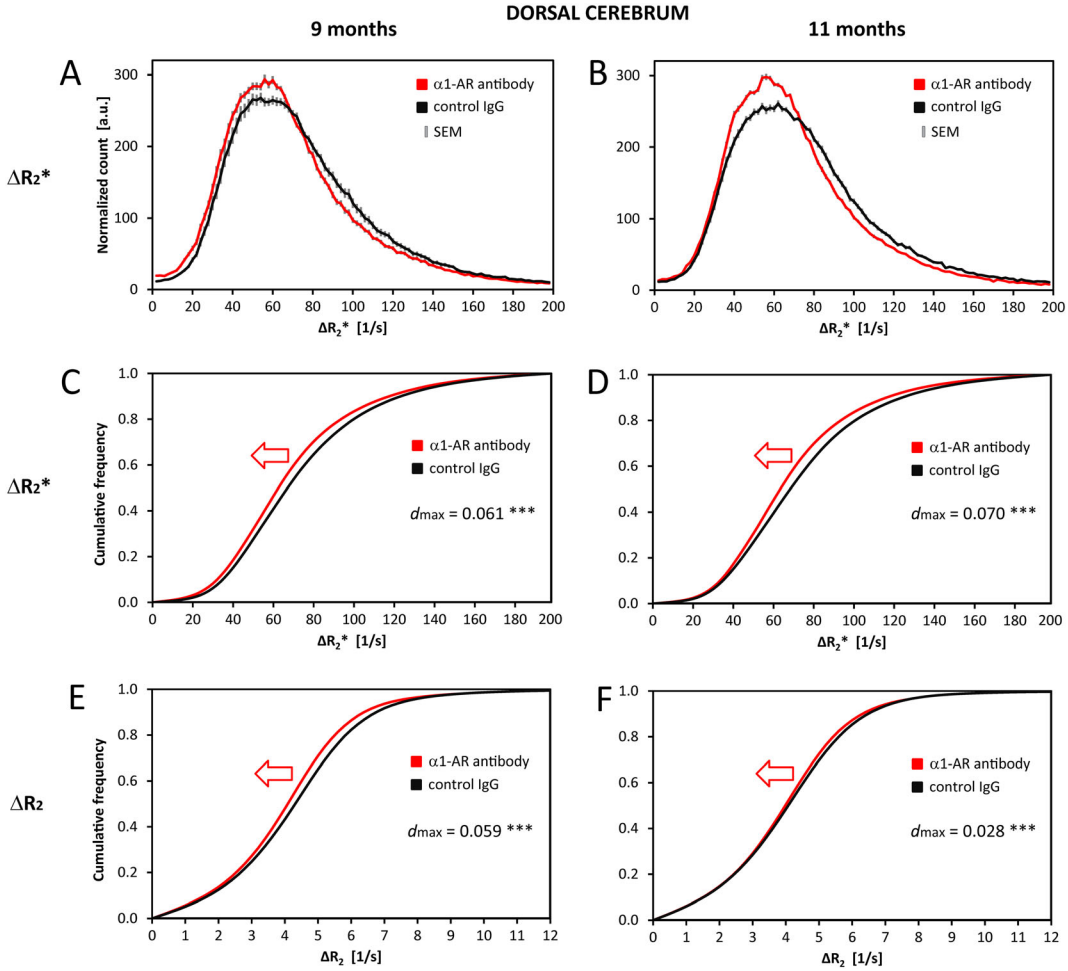

Figure 3. (A, B) Histograms of ΔR_2* in the dorsal cerebrum at 9 months (A) and 11 months (B) after treatment began. Mean ± standard error of the mean (SEM) for the α_1-adrenoceptor (α_1-AR) antibody group (red) and the control immunoglobulin G (IgG) group (black). At both time points, the histogram counts above $\Delta R_2^* \approx 75$ ms are decreased in the α_1-AR antibody group compared with the control group, whereas counts below $\Delta R_2^* \approx 75$ ms are increased. This translates into a shift of ΔR_2* towards lower values. (C, D) Corresponding plots of the cumulative frequency of ΔR_2* in the dorsal brain at 9 months (C) and 11 months (D). (E,F) Cumulative frequency of ΔR_2 in the dorsal brain at 9 months (E) and 11 months (F). (C–F) The leftward shift of the cumulative frequencies represents a significant reduction in ΔR_2* and ΔR_2 in the dorsal cerebrum with $^{***}p < 0.001$. d_{max} is the supremum of the absolute differences between the cumulative frequencies of both groups.

control IgG group ($p < 0.001$). The maximum differences d_{max} between the cumulative frequency of both groups at 11 months were 7.0% and 2.8% for ΔR_2* and ΔR_2, respectively.

A similar shift towards lower ΔR_2* and ΔR_2 in the α_1-AR antibody group was observed in the cortex (Fig. 4A–D) and hippocampus (Fig. 4E–H) at both time points ($p < 0.001$), with the exception of ΔR_2 in the hippocampus at 11 months. d_{max} values for the cortex at 11 months were larger (ΔR_2*, 8.3%; ΔR_2, 3.4%) than for the entire dorsal cerebrum. In the hippocampus, d_{max} for ΔR_2* (8.8%) was even higher, but d_{max} for ΔR_2 (0.3%) was smaller and non-significant.

Blood vessel immunofluorescent staining

Blood vessel immunofluorescent staining showed a strongly reduced CD31 staining in the cortex of animals exposed to the α_1-AR antibody (Fig. 5A, bottom panel) relative to the IgG controls (Fig. 5A, top panel). Quantitative analysis of the immunofluorescence images indicated a significant decrease in $CD31^+$ vessel area (56%, $p < 0.05$; Fig. 5B), i.e. the area fraction with positive CD31 staining for the α_1-AR antibody compared with the IgG controls. The CD31 cluster density (Fig. 5C) and CD31 cluster size (Fig. 5D) were reduced in the α_1-AR antibody group by 44% and 27%, respectively (both non-significant).

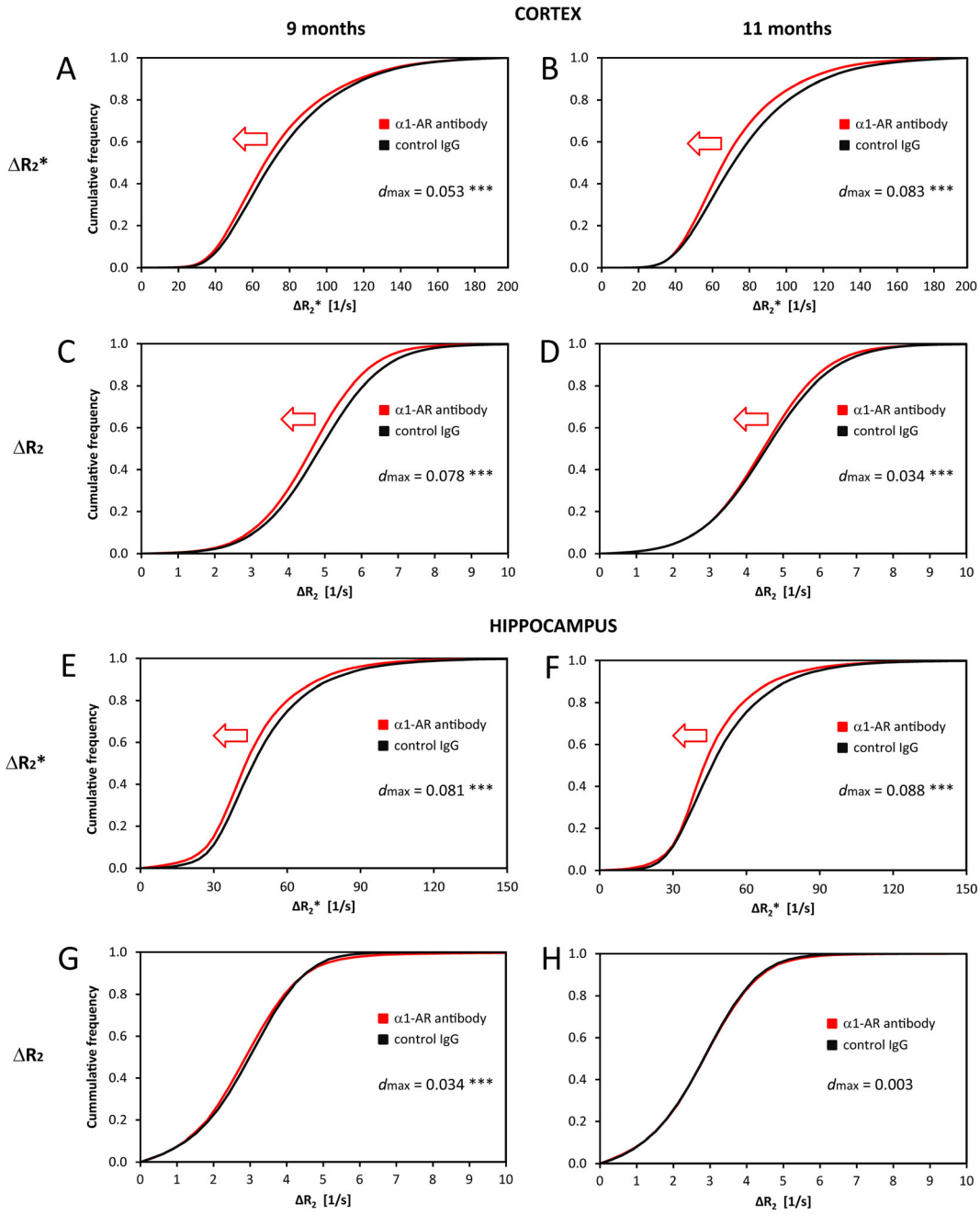

Figure 4. Cumulative frequencies of ΔR_2* (A, B, E, F) and ΔR_2 (C, D, G, H) in the cortex (A–D) and hippocampus (E–H) at 9 months (A, C, E, G) and 11 months (B, D, F, H) after treatment began. Mean for the α_1-adrenoceptor (α_1-AR) antibody group (red) and the control immunoglobulin G (IgG) group (black). A significant reduction in ΔR_2* and ΔR_2 (***$p < 0.001$) was observed in both cortex and hippocampus at all time points, with the exception of ΔR_2 in the hippocampus at 11 months. d_{max} is the supremum of the absolute differences between the cumulative frequencies of both groups.

NMR IN BIOMEDICINE

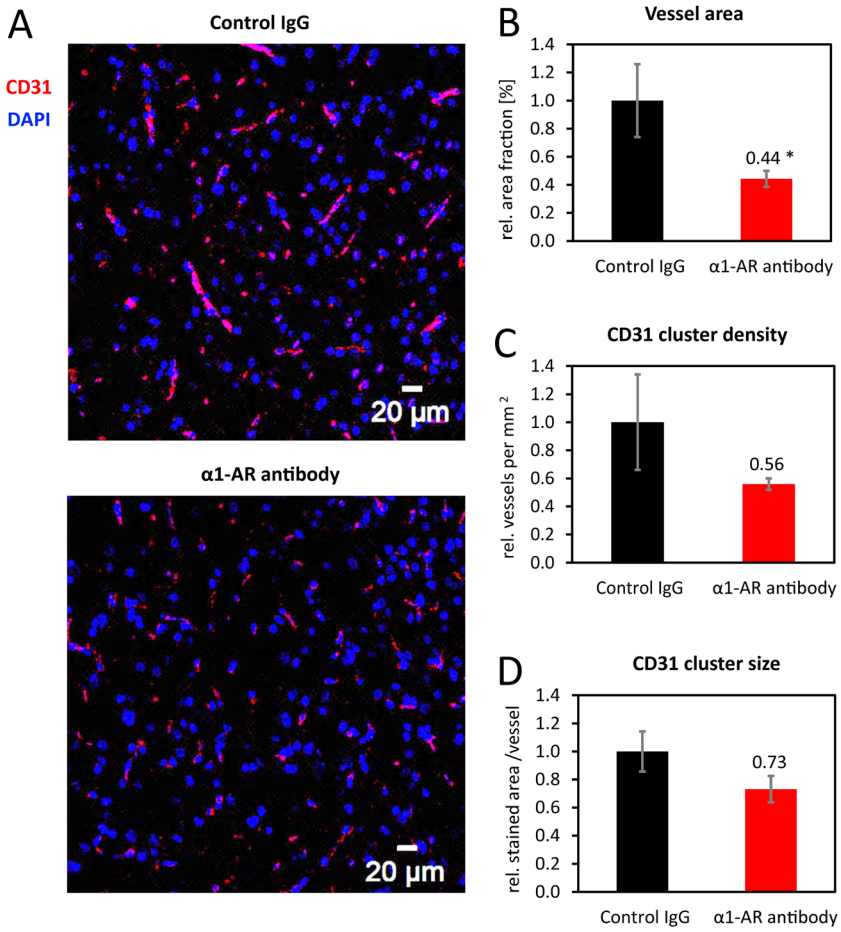

Figure 5. Blood vessel immunofluorescent staining with CD31 and 4′,6-diamidino-2-phenylindole (DAPI) (A). CD31 staining was strongly reduced in the cortex of animals exposed to the α_1-adrenoceptor (α_1-AR) antibody (bottom) compared with the immunoglobulin G (IgG) controls (top). Quantitative analysis of the immunofluorescence images indicated a significant ($^*p < 0.05$) decrease of 56% in the vessel area (B), i.e. the area fraction with positive CD31 staining for the α_1-AR antibody (red) relative to the IgG controls (black). CD31 cluster density (C) and CD31 cluster size (D) were reduced in the α_1-AR antibody group by 44% and 27%, respectively.

DISCUSSION

Ferumoxytol particle size analysis and dose optimization

The particle size analysis of different Feraheme® vials showed that ferumoxytol's average colloidal particle size is 23.38 ± 0.37 nm (instrument accuracy, ±2%) and hence 22% smaller than the commonly cited 30 nm (15). More importantly, the average size variation between batches was very small (standard deviation, 1.6%; instrument precision, ±2%) and the samples were monomodal (i.e. only one peak) and monodisperse (i.e. very narrow width of distribution). These are prerequisites for use as an intravascular contrast agent in rCBV studies, as the magnetic properties of USPIOs depend on their particle size (14).

The subsequent pilot MRI experiments demonstrated that the use of ferumoxytol as an intravascular contrast agent for rat rCBV mapping at 9.4 T is feasible: increasing doses of ferumoxytol led to a strong decrease in T_2* and T_2 of rat brains, which could easily be detected with T_2*(T_2)-weighted MRI and T_2*(T_2) mapping. With increasing iron dose, a linear rise in R_2* and sublinear rise in R_2 were observed, which is in agreement with previous findings for AMI-227 (Sinerem®, Guerbet, France), an USPIO contrast agent of similar size (30). For CBV estimation based on single-echo T_2*- or T_2-weighted imaging, an optimal iron dose can be derived from contrast-to-noise measurements (31). However, no equivalent approach exists for multi-echo parametric mapping of T_2* and T_2, as employed in this study. Balancing the constraints of the signal-to-noise ratio of the first five gradient echo images (TE = 2.1–10.7 ms), which decreases with increasing ferumoxytol dose, and rCBV measurement sensitivity, which increases with ferumoxytol dose, a dose of 10 mg Fe/kg was chosen for the rCBV measurements. This dose is slightly higher than the 3.8–9.0 mg Fe/kg dose that has been used previously for rat rCBV measurements at 11.75 T (16,27,28).

The advantage of the slow washout of ferumoxytol is that MR image acquisitions post-injection do not need to be started with 'second' precision: for instance, during a 30-s delay, cortical R_2* and R_2 will increase by less than 0.1%. Ferumoxytol's sufficiently high relaxivities and iron concentration allow for small volume doses. All these characteristics indicate that ferumoxytol is well suited as an intravascular contrast agent for longitudinal rCBV studies in rats at 9.4 T.

rCBV in α_1-AR antibody-exposed animals *versus* controls

Ferumoxytol-enhanced steady-state rCBV estimation revealed significant differences in the relaxivities ΔR_2* and ΔR_2 of α_1-AR antibody-exposed rats relative to the control group. Although the differences were small, the statistical analysis showed

that the chance of obtaining such differences between two random groups from the naïve animal population were very small ($p < 0.001$; see also the small SEMs in Fig. 3A, B or compare with the non-significant group difference shown in Fig. 4H). α_1-AR antibodies induced a widespread rCBV reduction, observed as reductions in the cerebral ΔR_2* and ΔR_2 at 9 and 11 months of treatment. More detailed analysis of the subregions within the cerebrum showed similarly large effects in the cortex and hippocampus, which are important in the context of dementia. α_1-ARs are found in the hippocampus, where animal studies have shown the ability of α_1-AR agents to modulate long-term potentiation and memory (32). However, the precise distribution of α_1-AR expression and its subtypes in the human brain are unknown, making functional comparisons challenging (33). It remains to be clarified whether the observed impacts of α_1-AR antibodies on rCBV in rats are associated with impairments in cognitive function, which is possible as the same antibodies have also been detected in patients with Alzheimer's disease with cerebrovascular disease (34), where it has been suggested that the vascular symptoms could be induced by the α_1-AR antibody (7,8). As the ΔR_2*-based rCBV effects are of similar magnitude in the cortex and hippocampus as in the entire dorsal cerebrum, effects in these subregions must be accompanied by rCBV reductions in other subregions of the dorsal cerebrum.

ΔR_2*-based and ΔR_2-based rCBV estimates showed some dissimilarities, for instance ΔR_2* but not ΔR_2 was significantly reduced in the hippocampus. Dissimilar findings in ΔR_2* and ΔR_2 might be explained by their respective dependences on the size and structure of the vascular compartment (17,30), which was also the motivation for measuring both parameters in this study. Although the USPIO-induced magnetic field inhomogeneity within voxels results directly in a ΔR_2* decrease as a result of reversible spin dephasing, the USPIO effect on ΔR_2 depends on the intravascular–extravascular diffusional motion of water creating irreversible spin dephasing. This translates into rather different vessel size dependences, with ΔR_2* having similar sensitivity to all vessel sizes and ΔR_2 being predominantly sensitive to small arterioles, venules and capillaries of the brain (17). It should also be noted that ΔR_2 might be underestimated as a result of using a multi-echo, spin-echo protocol with short inter-echo times of 10 ms, which interferes with the effective water diffusion contribution (14,35).

Moreover, in addition to the desired dependence of the transverse relaxivities on the vascular volume fraction and contrast agent concentration, variations in hematocrit are a potentially confounding factor. USPIOs are only present in the plasma volume fraction of the blood and not in the erythrocyte volume fraction. Hence, USPIO-enhanced MRI estimates cerebral plasma volume rather than blood volume. The hematocrit is known to be lower in the microvasculature because of plasma skimming (36), which translates into a larger plasma volume fraction and hence a higher USPIO blood concentration. Blood volume (and its changes) at the capillary level may therefore be overestimated when compared with larger vessels.

Although we observed a significant α_1-AR antibody impact on cortical ΔR_2* and ΔR_2, in the hippocampus, ΔR_2*, but not ΔR_2, was reduced. Keeping in mind the different vessel size dependence of ΔR_2* and ΔR_2, this might be caused by a different balance between α_1-AR antibody effects in small and large vessels in the hippocampus, but the mechanisms behind these findings remain to be unraveled.

The anesthetic's known intrinsic vasodilatory action may have led to a global increase in CBV (37,38). This effect may have translated into a global overestimation of CBV for the animals of both groups, but we cannot rule out that it may also have contributed to the differentiation of both groups if the α_1-AR antibody also impacted on the dilatory ability of the vasculature, i.e. the cerebrovascular reactivity (CVR). Conceivably, isoflurane anesthesia could be interpreted as a vasodilatory challenge, resulting in CBV and CVR effects of the α_1-AR antibody causing the observed rCBV group differences.

ΔR_2* reflects the local USPIO blood plasma concentration, but it can only be a surrogate of CBV as the exact blood concentration of the contrast agent is unknown and may vary slightly between experiments and also within the vasculature because of its dependence on hematocrit. Inter- and intra-subject variations in blood concentration may be accounted for by the normalization of ΔR_2* to a reference region that is known to be insensitive to the treatment; however, this approach was not applicable here because of the systemic impact of the α_1-AR autoantibody. To adjust the contrast agent dose, the body weight was used as a surrogate of blood/plasma volume. The relationship between body weight and blood/plasma volume is very close: for Wistar rats, above 120 g body weight, the linear correlation is highly significant ($r = 0.99$, $n = 70$) (39). Moreover, in this study, body weight was not significantly different between groups (e.g. 691 ± 17 g *versus* 677 ± 32 g, $p = 0.70$ at 9 months of treatment).

The MRI results prompted us to investigate whether the observed rCBV changes were reflected in changes in the cerebral blood vessels. We hypothesized that *in vivo* rCBV findings at the final time point would correlate with *ex vivo* immunohistological analyses of α_1-AR antibody-induced blood vessel impairments. After the last MRI time point, the rats were sacrificed and brain sections were analyzed with immunostaining. Quantitative analysis indeed showed significantly less $CD31^+$ blood vessel signal in the cerebral cortex of the α_1-AR group. Although these microscopic *ex vivo* data showed a larger relative effect, rCBV is a macroscopic method that has been proven to have sufficient sensitivity to detect such rCBV effects *in vivo* and non-invasively. The *ex vivo* results support our *in vivo* rCBV measurements, rule out that this was an entirely CVR-based effect and confirm deficiencies of the cerebral microvasculature in animals exposed to the α_1-AR antibody, which can be quantified non-invasively by MRI rCBV estimation.

CONCLUSIONS

The estimation of CBV by ferumoxytol-enhanced steady-state MRI at 9.4 T was successfully established and revealed a significant negative impact of α_1-adrenergic receptor antibodies on the cerebral microvasculature. rCBV was reduced in the cortex, hippocampus and, beyond that, in the dorsal cerebrum. Immunohistological analyses confirmed α_1-AR antibody-induced blood vessel deficiencies. These findings confirm the hypothesis that the α_1-AR antibody has effects reaching beyond previously reported macrovascular impairments in the predominantly extracranial major draining vessels of the rat brain (11) and leads to cerebral microvessel damage throughout the brain. This further underlines the suggested significance of this antibody in brain diseases linked to vasculature impairments, such as dementia.

Acknowledgements

This work was supported by the ProFIT program of the European Community (grant no. 10145576 to MB).

REFERENCES

1. Pantoni L. Cerebral small vessel disease: from pathogenesis and clinical characteristics to therapeutic challenges. Lancet Neurol. 2010; 9(7): 689–701.
2. Yarchoan M, Xie SX, Kling MA, Toledo JB, Wolk DA, Lee EB, Van Deerlin V, Lee VM, Trojanowski JQ, Arnold SE. Cerebrovascular atherosclerosis correlates with Alzheimer pathology in neurodegenerative dementias. Brain 2012; 135(Pt 12): 3749–3756.
3. Hunter JM, Kwan J, Malek-Ahmadi M, Maarouf CL, Kokjohn TA, Belden C, Sabbagh MN, Beach TG, Roher AE. Morphological and pathological evolution of the brain microcirculation in aging and Alzheimer's disease. PLoS One 2012; 7(5): e36893.
4. Fu ML, Herlitz H, Wallukat G, Hilme E, Hedner T, Hoebeke J, Hjalmarson A. Functional autoimmune epitope on alpha 1-adrenergic receptors in patients with malignant hypertension. Lancet 1994; 344(8938): 1660–1663.
5. Yan L, Xu Y, Yao H, Xue W, Tian J, Ren H, Wu Y, Yang G, Ma XL, Liu H. The effects of autoantibodies against the second extracellular loop of alpha(1)-adrenoceptor on vasoconstriction. Basic Res. Cardiol. 2009; 104(5): 581–589.
6. Karczewski P, Hempel P, Kunze R, Bimmler M. Agonistic autoantibodies to the alpha(1)-adrenergic receptor and the beta(2)-adrenergic receptor in Alzheimer's and vascular dementia. Scand. J. Immunol. 2012; 75(5): 524–530.
7. Zhou Z, Liao Y, Li L, Wei F, Wang B, Wei Y, Wang M, Cheng X. Vascular damages in rats immunized by alpha1-adrenoceptor peptides. Cell. Mol. Immunol. 2008; 5(5): 349–356.
8. Wenzel K, Haase H, Wallukat G, Derer W, Bartel S, Homuth V, Herse F, Hubner N, Schulz H, Janczikowski M, Lindschau C, Schroeder C, Verlohren S, Morano I, Muller DN, Luft FC, Dietz R, Dechend R, Karczewski P. Potential relevance of alpha(1)-adrenergic receptor autoantibodies in refractory hypertension. PLoS One 2008; 3(11): e3742.
9. Xia Y, Kellems RE. Receptor-activating autoantibodies and disease: preeclampsia and beyond. Expert Rev. Clin. Immunol. 2011; 7(5): 659–674.
10. O'Neill C, Fowler CJ, Marcusson JO, Winblad B. Adrenergic, serotoninergic, histaminergic, and imipramine binding sites in postmortal human cerebral microvessel preparations. J. Neural Transm. 1988; 73(3): 177–189.
11. Karczewski P, Pohlmann A, Wagenhaus B, Wisbrun N, Hempel P, Lemke B, Kunze R, Niendorf T, Bimmler M. Antibodies to the alpha1-adrenergic receptor cause vascular impairments in rat brain as demonstrated by magnetic resonance angiography. PLoS One 2012; 7(7): e41602.
12. Zaharchuk G. Theoretical basis of hemodynamic MR imaging techniques to measure cerebral blood volume, cerebral blood flow, and permeability. Am. J. Neuroradiol. 2007; 28(10): 1850–1858.
13. Christen T, Ni W, Qiu D, Schmiedeskamp H, Bammer R, Moseley M, Zaharchuk G. High-resolution cerebral blood volume imaging in humans using the blood pool contrast agent ferumoxytol. Magn. Reson. Med. 2013; 70(3): 705–710.
14. Kim SG, Harel N, Jin T, Kim T, Lee P, Zhao F. Cerebral blood volume MRI with intravascular superparamagnetic iron oxide nanoparticles. NMR Biomed. 2013; 26(8): 949–962.
15. Weinstein JS, Varallyay CG, Dosa E, Gahramanov S, Hamilton B, Rooney WD, Muldoon LL, Neuwelt EA. Superparamagnetic iron oxide nanoparticles: diagnostic magnetic resonance imaging and potential therapeutic applications in neurooncology and central nervous system inflammatory pathologies, a review. J. Cereb. Blood Flow Metab. 2010; 30(1): 15–35.
16. Gahramanov S, Muldoon LL, Li X, Neuwelt EA. Improved perfusion MR imaging assessment of intracerebral tumor blood volume and antiangiogenic therapy efficacy in a rat model with ferumoxytol. Radiology 2011; 261(3): 796–804.
17. Boxerman JL, Hamberg LM, Rosen BR, Weisskoff RM. MR contrast due to intravascular magnetic susceptibility perturbations. Magn. Reson. Med. 1995; 34(4): 555–566.
18. Mandeville JB, Marota JJ, Kosofsky BE, Keltner JR, Weissleder R, Rosen BR, Weisskoff RM. Dynamic functional imaging of relative cerebral blood volume during rat forepaw stimulation. Magn. Reson. Med. 1998; 39(4): 615–624.
19. Weisskoff RM, Zuo CS, Boxerman JL, Rosen BR. Microscopic susceptibility variation and transverse relaxation: theory and experiment. Magn. Reson. Med. 1994; 31(6): 601–610.
20. Shi Q, Pisani LJ, Lee YK, Messing S, Ansari C, Bhaumik S, Lowery L, Lee BD, Meyer DE, Daldrup-Link HE. Evaluation of the novel USPIO GEH121333 for MR imaging of cancer immune responses. Contrast Media Mol. Imaging 2013; 8(3): 281–288.
21. Lu M, Cohen MH, Rieves D, Pazdur R. FDA report: ferumoxytol for intravenous iron therapy in adult patients with chronic kidney disease. Am. J. Hematol. 2010; 85(5): 315–319.
22. Pannetier N, Lemasson B, Christen T, Tachrount M, Tropres I, Farion R, Segebarth C, Remy C, Barbier EL. Vessel size index measurements in a rat model of glioma: comparison of the dynamic (Gd) and steady-state (iron-oxide) susceptibility contrast MRI approaches. NMR Biomed. 2012; 25(2): 218–226.
23. Qiu D, Zaharchuk G, Christen T, Ni WW, Moseley ME. Contrast-enhanced functional blood volume imaging (CE-fBVI): enhanced sensitivity for brain activation in humans using the ultrasmall superparamagnetic iron oxide agent ferumoxytol. Neuroimage 2012; 62(3): 1726–1731.
24. Varallyay CG, Nesbit E, Fu R, Gahramanov S, Moloney B, Earl E, Muldoon LL, Li X, Rooney WD, Neuwelt EA. High-resolution steady-state cerebral blood volume maps in patients with central nervous system neoplasms using ferumoxytol, a superparamagnetic iron oxide nanoparticle. J. Cereb. Blood Flow Metab. 2013; 33(5): 780–786.
25. Thompson EM, Guillaume DJ, Dosa E, Li X, Nazemi KJ, Gahramanov S, Hamilton BE, Neuwelt EA. Dual contrast perfusion MRI in a single imaging session for assessment of pediatric brain tumors. J. Neurooncol 2012; 109(1): 105–114.
26. Farrell BT, Hamilton BE, Dosa E, Rimely E, Nasseri M, Gahramanov S, Lacy CA, Frenkel EP, Doolittle ND, Jacobs PM, Neuwelt EA. Using iron oxide nanoparticles to diagnose CNS inflammatory diseases and PCNSL. Neurology 2013; 81(3): 256–263.
27. Muldoon LL, Gahramanov S, Li X, Marshall DJ, Kraemer DF, Neuwelt EA. Dynamic magnetic resonance imaging assessment of vascular targeting agent effects in rat intracerebral tumor models. Neuro-Oncology 2011; 13(1): 51–60.
28. Varallyay CG, Muldoon LL, Gahramanov S, Wu YJ, Goodman JA, Li X, Pike MM, Neuwelt EA. Dynamic MRI using iron oxide nanoparticles to assess early vascular effects of antiangiogenic versus corticosteroid treatment in a glioma model. J. Cereb. Blood Flow Metab. 2009; 29(4): 853–860.
29. Muldoon LL, Sandor M, Pinkston KE, Neuwelt EA. Imaging, distribution, and toxicity of superparamagnetic iron oxide magnetic resonance nanoparticles in the rat brain and intracerebral tumor. Neurosurgery 2005; 57(4): 785–796; discussion 785–796.
30. Tropres I, Grimault S, Vaeth A, Grillon E, Julien C, Payen JF, Lamalle L, Decorps M. Vessel size imaging. Magn. Reson. Med. 2001; 45(3): 397–408.
31. Mandeville JB. IRON fMRI measurements of CBV and implications for BOLD signal. Neuroimage 2012; 62(2): 1000–1008.
32. Sirvio J, MacDonald E. Central alpha1-adrenoceptors: their role in the modulation of attention and memory formation. Pharmacol. Ther. 1999; 83(1): 49–65.
33. Szot P, White SS, Greenup JL, Leverenz JB, Peskind ER, Raskind MA. Alpha1-adrenoreceptor in human hippocampus: binding and receptor subtype mRNA expression. Brain Res. Mol. Brain Res. 2005; 139(2): 367–371.
34. Lopez OL, Rabin BS, Huff FJ, Rezek D, Reinmuth OM. Serum autoantibodies in patients with Alzheimer's disease and vascular dementia and in nondemented control subjects. Stroke 1992; 23(8): 1078–1083.
35. Boehm-Sturm P, Farr TD, Adamczak J, Jikeli JF, Mengler L, Wiedermann D, Kallur T, Kiselev V, Hoehn M. Vascular changes after stroke in the rat: a longitudinal study using optimized magnetic resonance imaging. Contrast Media Mol. Imaging 2013; 8(5): 383–392.
36. Perkkio J, Keskinen R. Hematocrit reduction in bifurcations due to plasma skimming. Bull. Math. Biol. 1983; 45(1): 41–50.
37. Matta BF, Heath KJ, Tipping K, Summors AC. Direct cerebral vasodilatory effects of sevoflurane and isoflurane. Anesthesiology 1999; 91(3): 677–680.
38. Hendrich KS, Kochanek PM, Melick JA, Schiding JK, Statler KD, Williams DS, Marion DW, Ho C. Cerebral perfusion during anesthesia with fentanyl, isoflurane, or pentobarbital in normal rats studied by arterial spin-labeled MRI. Magn. Reson. Med. 2001; 46(1): 202–206.
39. Lee HB, Blaufox MD. Blood volume in the rat. J. Nucl. Med. 1985; 26(1): 72–76.

SUPPORTING INFORMATION

Additional supporting information may be found in the online version of this article at the publisher's web site.